LES Investigation of Aerodynamics Performance in an Axial Compressor Stage

Gaofeng Wang[1], Stéphane Moreau[1], Florent Duchaine[2], Jerome de Laborderie[2], and Laurent Gicquel[2]

[1] *Université de Sherbrooke*
Sherbrooke, QC J1K 2R1, Canada

[2] *CFD team CERFACS*
42 avenue Gaspard Coriolis, 31057 Toulouse Cedex 1, France

Email: *gaofeng.wang@usherbrooke.ca*

ABSTRACT

An axial compressor stage (the so called CME2 stage; Re = 700,000 and Mach Number = 0.5) is simulated by an unstructured LES code, TurboAVBP. This industry-relevant configuration has been well investigated by several RANS (Reynolds Averaged Navier-Stokes) simulations with quite acceptable computation costs, though the limitations of RANS models are evidenced in evaluating secondary flow losses (including boundary layer transition, tip corner vortex, hub corner vortex and wake mixings), which are industrial targets for optimizations nowadays. Three LES results using three different codes, including two pioneering LES simulations with structured meshes on this compressor (Laborderie et. al. AIAA2013 and Gourdain, ASME2013), are compared together on the mean and unsteady components of the flow with the previous Unsteady RANS predictions and experimental data. LES is proven to be a very promising tool for the predictions of unsteady complex turbulent flow in a turbomachinery stage. The LES results show natural transitions from laminar to turbulence at mid-chord for suction sides of both rotor blades and stator vanes, which lead to thinner boundary layers than URANS. The predictions of secondary flow structures are compared, showing the tolerance ranges of the simulations. Most noticeably the large flow separation predicted by URANS simulations over 25% of the blade span of the stator vanes from the hub is significantly reduced or totally suppressed. Both flow modifications yield significantly different overall flow performances stressing the importance and the relevance of LES modeling in turbomachinery applications.

1 INTRODUCTION

The compressor is one of three core components of a gas turbine and is designed to increase the pressure of intaking air for a high power density performance. The flow successively goes around the rotating rotor blades and fixed stator vanes, converts the velocity energy into pressure energy. This turbomachinery flow is inherently unsteady and turbulent with rather complex three-dimensional aerodynamic phenomena characterized by boundary layer effects, secondary flows generated by the passage pressure gradients, and vortical flow structures such as the leading edge horseshoe vortices, tip-leakage flow vortices and corner vortices [7]. An accurate representation of these unsteady flow physics is required to understand the processes: (1) which lead to loss in seeking better overall performance; (2) which lead to aerodynamic instabilities (stall or surge) to avoid mechanical failure.

Although much more computationally intensive than the traditional Reynolds-Averaged Navier-Stokes (RANS) approach, Large Eddy Simulation (LES) can alleviate the modeling efforts, by explicitly resolving the temporal and spatial evolutions of large flow structures and by filtering out the smaller easier to model turbulent sub-grid structures. More and more efforts have been made on the predictions of these complex turbulent flows around isolated parts of turbomachines by use of the high-fidelity LES modeling approach (review by Tucker [30]). Preliminary demonstrations on some turbomachinery components show that LES can resolve flows with transitions, separations on structured or unstructured meshes [16, 2, 4, 18, 8]. Tip-clearance flow predictions have also been addressed successfully with LES [33, 34, 35]. McMullan *et. al.* [17] have also demonstrated that LES can accurately predict surface pressure on the turbomachinery cascade. A few LES simulations of compressor flows (Reynolds number varies from $0.15 \sim 6 \times 10^6$) are reviewed by Gourdain *et. al.* [12]. Nowadays, algorithmic developments complemented by high performance massively parallel machines allow having CFD LES solvers capable of handling billions of cells with a very reasonable speedup by making use of up to one million cpu cores at once [20, 1]. Following the analysis of Tucker [29] and Gourdain *et. al.* [12], HPC resource seems to be affordable in simulating most of the compressor

stages of gas turbine.

In the present study, the feasibility of LES simulation approach is applied to simulate an axial compressor stage CME2 using unstructured mesh for first time, which has been investigated by experiments at Laboratoire de Mecanique de Lille (LML) and Laboratoire d'Energetique et de Fluides Internes (LEFI) in France [9], by RANS simulations [10, 5]) and by LES simulations [11, 5] with structured mesh in literature. The paper is organized as follows: the numerical methods are firstly briefed in Section 2; the numerical setups is detailed in Section 3; the simulation results are presented and discussed in Section 4; finally, conclusion remarks are provided in Section 5.

2 NUMERICAL METHOD

Governing equations and numerical scheme

The filtered unsteady compressible Navier-Stokes equations for LES that describe the spatially filtered mass, momentum and energy $(\rho, \rho\mathbf{U}, \rho E)$ conservations, can be written in the following conservative form:

$$\frac{\partial \mathbf{W}}{\partial t} + \vec{\nabla} \cdot \vec{\mathcal{F}} = 0, \tag{1}$$

where $\mathbf{W}$ is the vector containing the conservative variables $(\rho, \rho\mathbf{U}, \rho E)^T$ and $\vec{\mathcal{F}} = (\mathbf{F}, \mathbf{G}, \mathbf{H})^T$ is the flux tensor. For convenience, the flux is divided into two components:

$$\vec{\mathcal{F}} = \vec{\mathcal{F}}^C(\mathbf{W}) + \vec{\mathcal{F}}^V(\mathbf{W}, \nabla\mathbf{W}) \tag{2}$$

where $\vec{\mathcal{F}}^C$ is the convective flux depending on $\mathbf{W}$ and $\vec{\mathcal{F}}^V$ is the viscous flux depending on both $\mathbf{W}$ and its gradients $\nabla\mathbf{W}$. The contributions of Sub-Grid Scale (SGS) turbulence models are included in the viscous flux through the addition of the so called turbulent viscosity ν_t. The present work relies on the Wall-Adapting Local Eddy-viscosity (WALE) SGS model [21] for which the turbulent viscosity is modeled by

$$\nu_t = (C_w\Delta)^2 \frac{(s^d_{ij}s^d_{ij})^{3/2}}{(\tilde{S}_{ij}\tilde{S}_{ij})^{5/2} + (s^d_{ij}s^d_{ij})^{5/4}} \tag{3}$$

$$s^d_{ij} = \frac{1}{2}(\tilde{g}^2_{ij} + \tilde{g}^2_{ji}) - \frac{1}{3}\tilde{g}^2_{kk}\delta_{ij} \tag{4}$$

where $\tilde{S}_{ij}$ denotes the resolved rate-of-strain tensor, $\tilde{g}_{ij}$ denotes the resolved velocity gradient, $C_w = 0.4929$ denotes model constant and Δ denotes the characteristic filter length (the cubic-root of the cell volume), corresponding to the local mesh cell size.

Within the parallel LES solver AVBP [28], the governing equations (Eq. 1) are discretized into cell-vertex formalism and solved by Lax-Wendroff (LW) finite volume scheme [15] with 2nd-order accuracy in time and space.

Rotor-stator interface

The rotor/stator coupling interface is based on overlapping grids approach, which is exchanging Dirichlet boundary conditions at the overlapped regions across the interface using TurboAVBP [32]. Hence, two or more instances of the unstructured LES solver AVBP each with their own computational domain and static Domain Decomposition Method (DDM) algorithm, are coupled through the parallel coupler OpenPALM [23]. In the simulation, the whole flow domain should initially be divided into several static and rotating parts. For rotating parts, the solver uses the moving-mesh approach [19] in the absolute frame of reference while the remaining unit simulates the flow in the stationary part in the same coordinate system. The interfaces between the two units involving rotating and non-rotating parts are coupled, as explained before with the overlapping grids by exchanging and interpolating the conservative variables wherever needed. To do so, an efficient distributed search algorithm is implemented in the coupler OpenPALM to locate the points in parallel partitioned mesh [26]. This coupling algorithm will then update at each time step the information and carry the interpolation from one MPI code to the next and vice-versa. Issues of numerical stability of the coupled solution and the well-posed problem are directly linked to the size of the overlapped region and the stencil of the schemes. One layer of vertices is required across the interface for the LW scheme here, according to the previous investigation [32]. This approach have been successfully applied in several numerical investigations [32, 31, 22, 25, 3].

3 NUMERICAL SETUP

The CME2 compressor [9] investigated here is a low pressure single stage axial compressor established and experimentally investigated at the Laboratoire de Mecanique de Lille and Laboratoire d'Energetique et de Fluides Internes in France. It has some typical applications, for example mounted on the low speed shaft side for a turbofan engine. As shown in Fig. 1, the compressor stage has 30 rotor blades followed by 40 stator vanes. The midspan chord lengths are 84 mm and 77 mm for the rotor blade and the stator vane respectively. The simulation configuration is $1/10th$ of the entire geometry, consists of 3 rotor blades and 4 stator vanes in a 36° sector. The simulation domain is 426 mm long, with a convergent shape: the hub radius is $R^I_H = 196.9\ mm$ at the inlet and $R^O_H = 214\ mm$ at the outlet; the casing radius is kept constant as $R_C = 275\ mm$. For normal conditions of design, the compressor operates in a subsonic regime. The axial inlet Mach number is around 0.33. The rotational speed is $\Omega_n = 6300\ RPM$, with the tip Mach number of 0.58. At the normal operating point, the mass flow rate is $Q_n = 11\ kg \cdot s^{-1}$ and the total-to-total pressure ratio is $\pi = 1.14$. The Reynolds

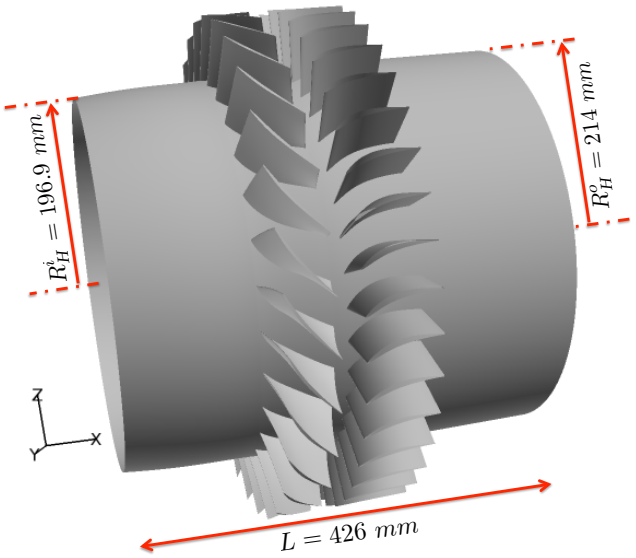

Figure 1: *The configuration of CME2 compressor.*

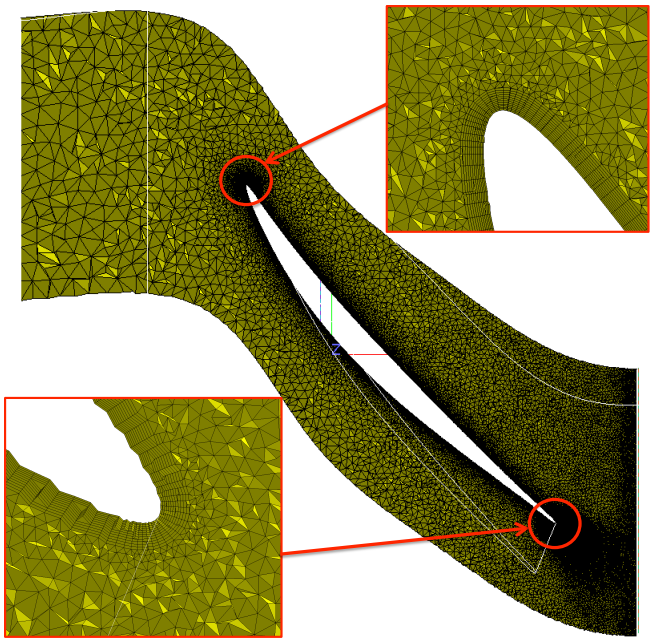

Figure 2: *The unstructured meshes for one rotor blade passage.*

number based on the rotor blade chord is about 7×10^5.

The computational domain consists of 245 million hybrid prismatic/tetrahedral cells and is separated into two parts: (1) the rotating part of the rotor; (2) the static part including both the inlet duct and the stator. Two parts are coupled through two overlapping interfaces. As illustrated in Fig. 2, the closing-wall region around the rotor blade is meshed by 12 layers of prism cells with initial height of 0.01 *mm* and expansion ratio of 1.2. The blade surface is discretized by triangular elements with the size of 0.35 *mm* in main region and 0.05 *mm* at the regions of the leading and trailing edges and the tip. The similar mesh topologies are used for the stator vanes. The meshes at casing and hub walls are tetrahedral cells with size of 0.5 *mm*.

The inlet and outlet boundaries are using Navier-Stokes Characteristic Boundary Conditions (NSCBC) [24]. A massflow profiles from the previous investigations is prescribed at the inlet. No turbulence fluctuations are imposed at the inflow. The outlet of the flow passage is prescribed by targeting a mean static pressure value using NSBC approach [13], which can capture the radial equilibrium naturally [14]. The solid walls of blades and vanes are modelled as nonslip adiabatic wall and a classical logarithmic wall-law boundary condition [27] is imposed at the hub and casing walls. The rotor mesh is rotating by a conventional moving grid method [19], while the rotor blades and the hub of this section are moving walls following the rotating movement. The two lateral surfaces delimiting the 36° sector in the azimuthal direction are axis-periodic boundaries.

According to the mesh refinement strategies, the time step is fixed to $\Delta t = 1 \times 10^{-8}$ s, which is controlled by the acoustic CFL number in the fully explicit solver. The simulation to cover one full 360° revolution requires 952 thousand iterations and costs about 1.8 million cpu hours (around one month of elapsed wall-clock time if using 2304 cores of a parallel platform).

4 RESULTS

The normalized wall normal distance y^+, constructed by an instantaneous field, is checked at first step in Fig. 3. In most of the region for both blade and vane surfaces, the dimensionless wall distance y^+ is at the region of 1 to 4 (may exceed 8 instantaneously at some limited area of the tip region and the leading edges), which indicates a good resolution at wall normal direction. For the streamwise and spanwise directions, $\Delta x = \Delta z = 35\Delta y = 35 \sim 120$. Generally, the mesh quality remains to be in an acceptable level to resolve the wall flow within reasonable computational costs.

Figure 4 pictures the main turbulent flow structures represented by the instantaneous iso-surface of Q-criterion. The iso-surface is colored by the mach number. Figure 4a shows the global structures of the turbulent flows within 3 rotor and 4 stator passages view from hub to casing. At the corner between each leading edges of the rotor blade and the hub, The horse-shoe vortex (A) occurs due to the rolling up effects of inflow boundary layer and develops into two legs on

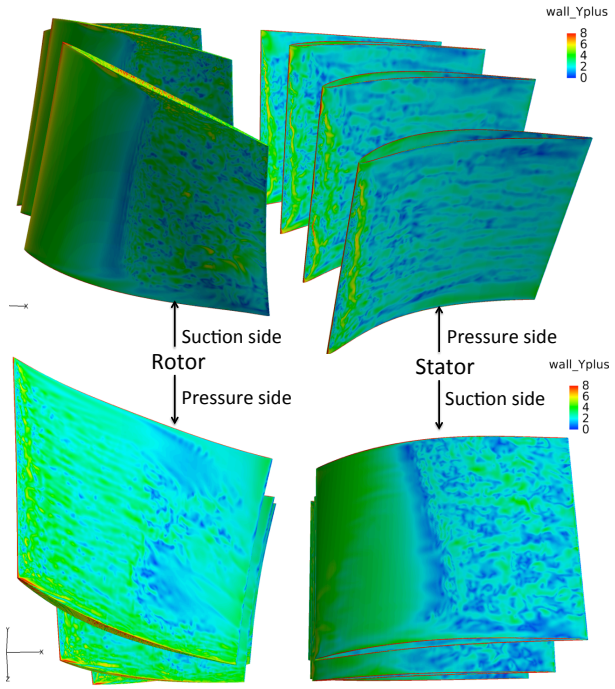

Figure 3: *The normalized wall distance y+.*

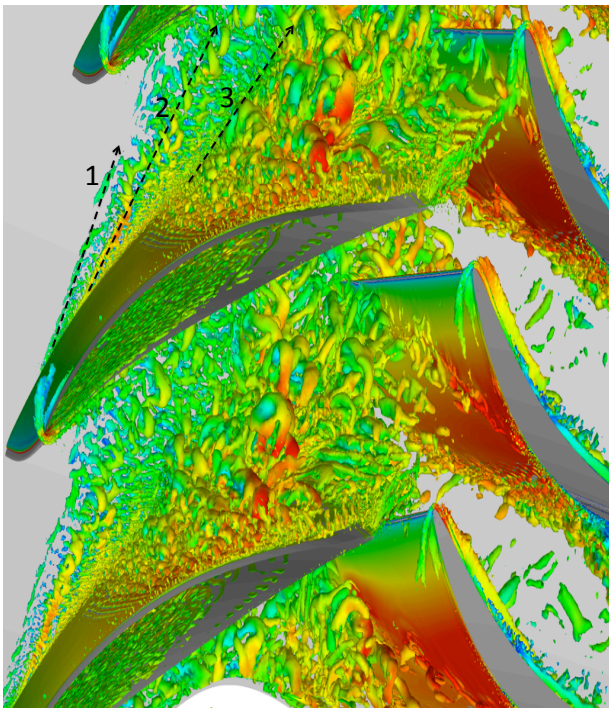

Figure 5: *Tip vortices structures: (1) induce vortex; (2) leakage vortex; (3) separation vortex.*

the pressure and suction sides respectively. The similar structures (E) are also found at the corners between stator vane and hub/casing walls. At the suction side of the rotor blade, the laminar boundary layer is kept at first half chord and then transitions to turbulent boundary layer (B) after mid-chord. At the stator suction side (Fig. 4b), the boundary layer is also seen starting the transitions from mid-chord (H) while the brushing of the incoming rotor wakes (D) do not trigger the transitions before mid-chord. At the positions after mid-chord, the rotor wake (I) is interacting with the turbulent boundary layer of the stator vane. The transitions of boundary layer start early at the pressure sides of both rotor and stator (F) due to leading edge effects. The tip vortices (C) are predicted at the position close to the casing, which consists of three vortex structures: leakage vortex, induced vortex and separation vortex shown in Fig. 5. The tip leakage vortex, originates at about 25% of the chord from the leading edge, is formed due to rolling-up of the leakage jet through the tip gap. The induced vortices are secondary vortices induced by the tip-leakage vortex at the upstream position. The flow separation of the leakage jet generates the tip separation vortices.

The velocity profiles at four axial planes are available by experimental investigations using LDA measurements [9]. Figure 6 displays the numerical predictions of mean axial velocity at the four planes. In $P1$ plane at the rotor inlet, the potential effect leads to a lower axial velocity at the regions approaching the leading edges. At the rotor exiting plane (P2), the wake is thinner than that predicted in RANS simulation [6, 10], which is more approaching the results from the experimental measurements [9] and the previous LES simulation by structured mesh [11, 5]. The low axial velocity at casing region in the middle of the passage is due to the developments of the tip vortices. A small boundary layer separation region may exists at the intersection region of the casing and the blade tip in pressure side. This pattern is then developing and passing through the coupled interface for the stator inlet (P3) plane. At the stator exit plane (P4), the velocity profile consists of a thin stator wake. Notice that only two tiny separation regions at the end wall of the suction side of the vane, while a large flow separation predicted by URANS simulations [10, 5] over 25% of the blade span of the stator vanes from the hub is significantly reduced or totally suppressed.

Figure 7 shows the averaged relative velocity and radical velocity at 5 spanwise locations of the rotor inlet plane. The LES results of the relative velocity profiles match better with experimental results [9] than the URANS predictions [6]. For the radial velocity components, LES predicts the similar profiles as the URANS simulations. Note that the relative velocity profiles are corrected by matching the operating inlet temperature conditions as the experiment. More quantitative comparisons between experiments data and LES statistics will be provided in near future.

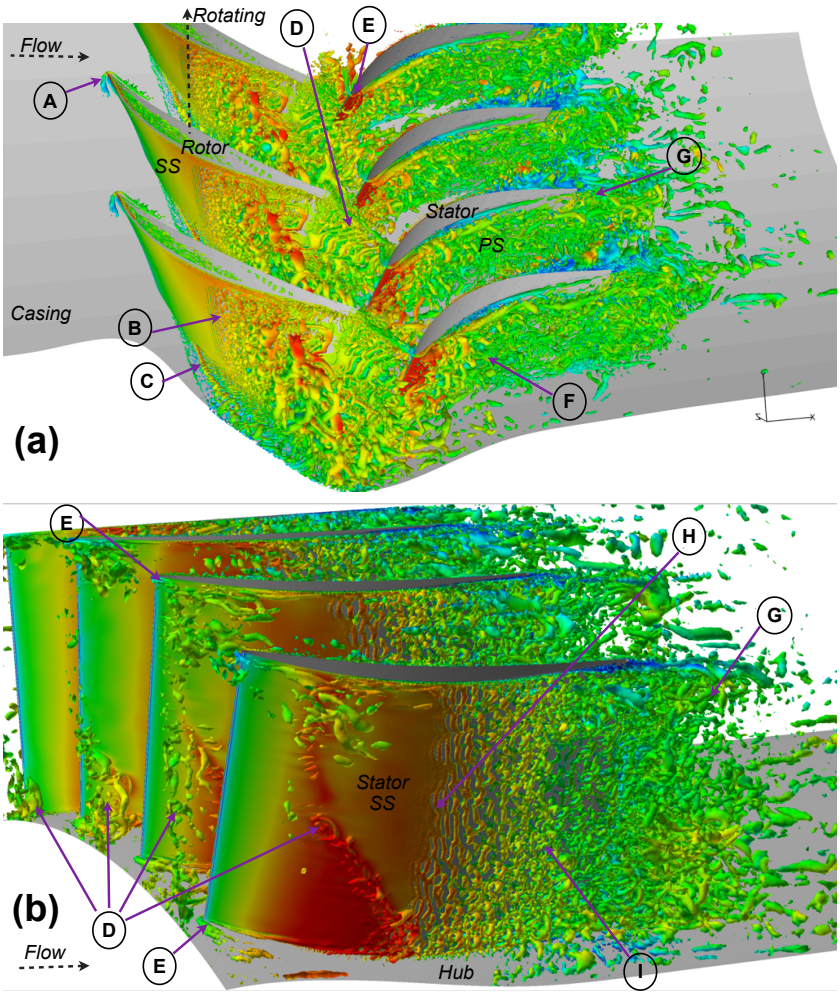

Figure 4: *Instantaneous iso-surface of Q-criterion colored by Mach number: (a) view from hub to casing; (b) view at suction side of stator. A, E - horseshoe vortex; B - transitions of boundary layer at rotor suction side; C - tip vortices; D - rotor wake mixing with turbulent boundary; F - turbulent boundary layer at stator pressure side; G - stator wake; H - transitions of boundary layer at stator suction side; I - rotor wake mixing with turbulent boundary layer at stator suction side.*

5 CONCLUSIONS

A low pressure single stage compressor, CME2, is simulated by an in-house unstructured LES code, TurboAVBP. The potential of LES for an accurate flow prediction of a compressor rotor/stator stage is illustrated. The inherently unsteady nature of LES allows capturing most of the unsteady flow structures: rotor-stator wake interactions, tip-clearance vortices, horse-shoe vortices, boundary layer transitions and separations, which are qualitatively matching with those experimental findings. Some mean LES statistics (relative velocity and radial velocity) are proven to be in reasonable agreements with experimental data and appear to be better than the URANS approach. Nevertheless the computational cost of the current wall-resolved computation, *i. e.* one month of computation on 2304 cpu cores for one full revolutions of the machine to get LES statistics (while optimizations are still possible) might be not affordable by the current industrial designs. More analysis of the details of flow physics are ongoing.

ACKNOWLEDGMENTS

The authors would like to thank the SAFRAN CN2020 Project and Mitacs Elevate Project for its financial support.

REFERENCES

[1] AVBP. Avbp code: www.cerfacs.fr/cfd/avbp_code.php and www.cerfacs.fr/cfd/cfdpublications.html, 2014.

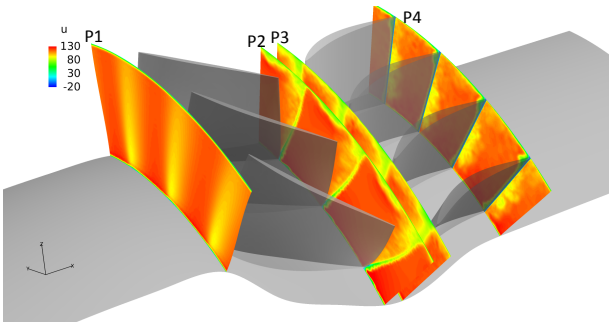

Figure 6: *The measurement planes at four axial positions colored by the mean axial velocity U.*

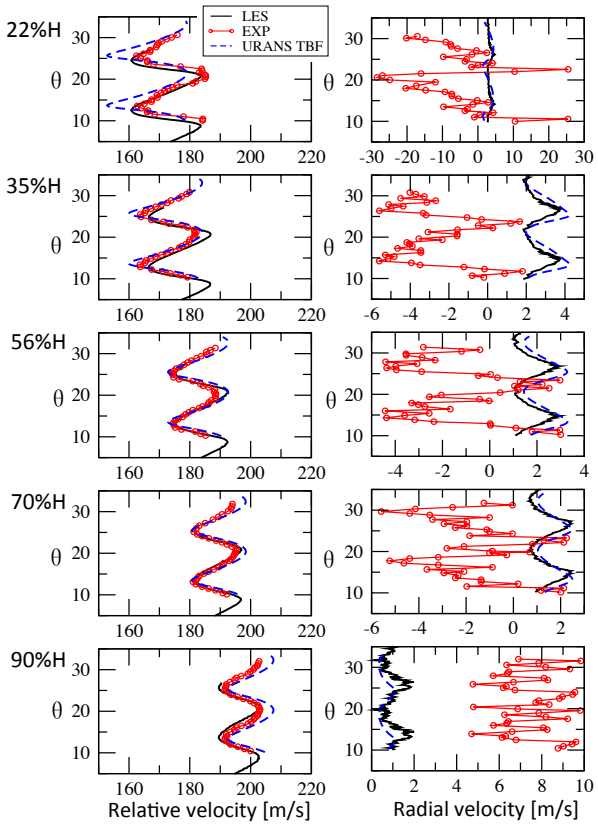

Figure 7: *The mean profile of numerical predictions of relative velocity and radial velocity at 5 span-wise locations of P1 plane.*

[2] R. Bhaskaran and S. K. Lele. Large eddy simulation of free-stream turbulence effects on heat transfer to a high-pressure turbine cascade. *Journal of Turbulence*, 11(6):1–15, 2010.

[3] A. Bonhomme, G. Wang, L. Selle, F. Duchaine, and T. Poinsot. A parallel multidomain coupled strategy to compute turbulent flows in fan-stirred bombs. *Computers and Fluids*, accepted, 2014.

[4] E. Collado-Morata, N. Gourdain, F. Duchaine, and L. Gicquel. Effects of free-stream turbulence on high pressure turbine blade heat transfer predicted by structured and unstructured les. *International Journal of Heat and Mass Transfer*, 55(21-22):5754 – 5768, 2012.

[5] J. de Laborderie, S. Moreau, and A. Berry. Compressor stage broadband noise prediction using a large-eddy simulation and comparisons with a cascade response model. In *19th AIAA/CEAS Aeroacoustics Conference*, pages AIAA–2013–2042, Berline, Germany, May 27-29, 2013.

[6] J. de Laborderie, L. Soulat, and S. Moreau. Prediction of noise sources in an axial compressor from a urans simulation. *Journal of Propulsion and Power*, Accepted, 2014.

[7] S. L. Dixon. *Fluid Mechanics, Thermodynamics of Turbomachinery*. Oxford: Butterworth-Heinemann Ltd., 1995.

[8] F. Duchaine, N. Maheau, V. Moureau, G. Balarac, and S. Moreau. Large eddy simulation and conjugate heat transfer around a low-mach turbine blade. *ASME TURBO EXPO GT2013-94257*, 2013.

[9] T. M. Faure, G.-J. Michon, H. Miton, and N. Vassilieff. Laser doppler anemometry measurements in an axial compressor stage. *Journal of Propulsion and Power*, 17:481–491, 2001.

[10] N. Gourdain. *Simulation numérique des phénomènes de décollement tournant dans les compresseurs axiaux*. PhD thesis, Ecole Centrale de Lyon, 2005.

[11] N. Gourdain. Validation of large-eddy simulation for the prediction of compressible flow in an axial compressor stage. In *ASME Turbo Expo 2013*, pages GT2013–94550, San Antonio, Texas, USA, June 3-7, 2013.

[12] N. Gourdain, F. Sicot, F. Duchaine, and L. Gicquel. Large eddy simulation of flows in industrial compressors: a path from 2015 to 2035. *Proceedings of the Royal Society A*, accepted, 2014.

[13] V. Granet, O. Vermorel, T. Leonard, L. Gicquel, , and T. Poinsot. Comparison of nonreflecting outlet boundary conditions for compressible solvers on unstructured grids. *AIAA Journal*, 48(10):2348–2364, 2010.

[14] C. Koupper, T. Poinsot, L. Gicquel, and F. Duchaine. Compatibility of characteristic boundary conditions with radial equilibrium in turbomachinery simulations. *AIAA Journal*, accepted, 2014.

[15] P. D. Lax and B. Wendroff. Difference schemes for hyperbolic equations with high order of accuracy. *Communications on pure and applied mathematics*, 17:381–398, 1964.

[16] K. Matsuura and C. Kato. Large eddy simulation of compressible transitional flows in a low-pressure turbine cascade. *AIAA Journal*, 45(2):442–457, 2007.

[17] W. McMullan and G. Page. Towards large eddy simulation of gas turbine compressors. *Progress in Aerospace Sciences*, 52(0):30 – 47, 2012.

[18] G. Medic, S. L. J. Joo, and O. Sharma. Prediction of heat transfer in a turbine cascade with high levels of free-stream turbulence. In *Proceeding of the Summer Program Center for Turbulence Research, NASA AMES - Stanford University, USA.*, 2012.

[19] V. Moureau, G. Lartigue, Y. Sommerer, C. Angelberger, O. Colin, and T. Poinsot. Numerical methods for unsteady compressible multi-component reacting flows on fixed and moving grids. *Journal of Computational Physics*, 202(2):710 – 736, 2005.

[20] J. W. Nichols, S. K. Lele, F. E. Ham, and J. E. Bridges. Prediction of supersonic jet noise using unstructred les: effects of chevrons. Technical report, Center for Turbulence Research, Stanford University, 2013.

[21] F. Nicoud and F. Ducros. Subgrid-scale stress modelling based on the square of the velocity gradient. *Flow, Turbulence and Combustion*, 62(3):183–200, 1999.

[22] D. Papadogiannis, F. Duchaine, F. Sicot, L. Gicquel, G. Wang, and S. Moreau. Large eddy simulation of a high pressure turbine stage: effects of sub-grid scale modelling and mesh resolution. In *ASME Turbo Expo 2013*, pages GT2014–25876, Dusseldorf, Germany, June 16-20, 2013.

[23] A. Piacentini, T. Morel, A. Thevenin, and F. Duchaine. Open-palm an open source dynamic parallel coupler. In *Coupled Problems 2011*, 2011.

[24] T. Poinsot and S. Lele. Boundary conditions for direct simulations of compressible viscous flows. *Journal of Computational Physics*, 101(1):104 – 129, 1992.

[25] A. Poubeau, R. Paoli, A. Dauptain, F. Duchaine, and G. Wang. Large eddy simulation of a solid rocket booster jet: towards a better prediction of the impact of solid-fuel launchers on the atmosphere. *AIAA Journal*, accepted, 2014.

[26] A. Refloch, B. Courbet, A. Murrone, P. Villedieu, C. Laurent, P. Gilbank, J. Troyes, L. Tessé, G. Chaineray, J. Dargaud, E. Quémerais, and F. Vuillot. Cfd platforms and coupling - cedre software. *The Onera Journal Aerospace Lab*, 2, 2011.

[27] P. Schmitt, T. Poinsot, B. Schuermans, and K. P. Geigle. Large-eddy simulation and experimental study of heat transfer, nitric oxide emissions and combustion instability in a swirled turbulent high-pressure burner. *Journal of Fluid Mechanics*, 570:17–46, 2007.

[28] T. Schonfeld and M. Rudgyardt. Steady and unsteady flow simulations using the hybrid flow solver avbp. *AIAA Journal*, 37:1378–1385, 1999.

[29] P. Tucker. Computation of unsteady turbomachinery flows: Part 1 "progress and challenges. *Progress in Aerospace Sciences*, 47(7):522 – 545, 2011.

[30] P. Tucker. Computation of unsteady turbomachinery flows: Part 2 "les and hybrids. *Progress in Aerospace Sciences*, 47(7):546 – 569, 2011.

[31] G. Wang, S. Moreau, F. Duchaine, N. Gourdain, and L. Gicquel. Large eddy simulations of the MT1 high-pressure turbine using TurboAVBP. In *Proceeding of 21st Annual Conference of the CFD Society of Canada*, Sherbrooke, Quebec, Canada, May 6-9, 2013.

[32] G. Wang, D. Papadogiannis, F. Duchaine, N. Gourdain, and L. Y. M. Gicquel. Towards massively parallel large eddy simulation of turbine stages. *ASME TURBO EXPO GT2013-94852*, 2013.

[33] D. You, R. Mittal, M. Wang, and P. Moin. Computational methodology for large-eddy simulation of tip-clearance flows. *AIAA Journal*, 42(2):271–279, 2004.

[34] D. You, M. Wang, P. Moin, and R. Mittal. Effects of tip-gap size on the tip-leakage flow in a turbomachinery cascade. *Physics of Fluids*, 18(105102), 2006.

[35] D. You, M. Wang, P. Moin, and R. Mittal. Large-eddy simulation analysis of mechanisms for viscous losses in a turbomachinery tip-clearance flow. *Journal of Fluid Mechanics*, 586:177–204, 2007.